the diagnostic pathology journal DIAGNOSTIC PATHOLOGY

Lavina Ahmed et al, diagnostic pathology 2016, 2:104
ISSN 2364-4893
DOI: http://dx.doi.org/10.17629/www.diagnosticpathology.eu-2016-2:104

Novel anti-human Axl monoclonal antibodies for improved patient biomarker studies

Lavina Ahmed[1,2], Sergej M. Kiprijanov[1], Hawa Nalwoga[2], Katarzyna Wnuk-Lipinska[1,4], Hallvard Haugen[1,4] James B. Lorens[1,2,4], Lars A. Akslen[2,3], David R. Micklem[1]*

Affiliation: [1]BerGenBio AS; Bergen, Norway; [2]Centre for Cancer Biomarkers CCBIO, Department of Clinical Medicine, University of Bergen; Bergen, Norway; [3]Department of Pathology, Haukeland University Hospital; Bergen, Norway; [4]Department of Biomedicine, University of Bergen; Bergen, Norway

* Corresponding author

E-mail address: david.micklem@bergenbio.com

Abstract

Background: Axl receptor tyrosine kinase has been associated with poor clinical outcome in a wide variety of malignancies including breast, lung, prostate, pancreatic, brain and myeloid cancers. Axl is up-regulated during tumour epithelial-to-mesenchymal transition (EMT) and is associated with metastasis, immune evasion and drug resistance.

Methods: The aim of this study was to develop improved assays for detection of Axl protein in patient samples. We developed a panel of mouse monoclonal antibodies directed against the extracellular domain of human Axl, from mice immunized with a recombinant antigen comprising the extracellular domains of human Axl fused to human IgG1 Fc domain. Anti-Axl monoclonal antibodies (MAbs) were assessed for sensitivity, specificity and utility using surface plasmon resonance (SPR) analysis, sandwich enzyme-linked immunosorbent assay (ELISA), Western blot analysis and immunohistochemistry (IHC) staining.

Results: One of the anti-human Axl MAb,1H12, performed particularly well, and SPR analysis confirmed both high affinity (50 pM) and high selectivity for Axl versus other Axl-family receptors. In IHC applications on selected human carcinomas and cancer cell line pellets, MAb 1H12 showed improved sensitivity and reduced background staining compared to other members of the MAb panel. A second MAb 5F11 showed very high affinity (5.8 pM) at a non-overlapping epitope and was selected as a partner for 1H12 in sandwich ELISA, producing a highly sensitive and specific assay.

Conclusion: MAbs 1H12 and 5F11 represent new anti-human Axl monoclonal antibodies for improved patient biomarker studies.

the diagnostic pathology journal DIAGNOSTIC PATHOLOGY

Lavina Ahmed et al, diagnostic pathology 2016, 2:104
ISSN 2364-4893
DOI: http://dx.doi.org/10.17629/www.diagnosticpathology.eu-2016-2:104

Keywords: Monoclonal antibodies, cancer, EMT, diagnostic biomarkers, Axl, ELISA, Biacore, IHC, Western blot.

Virtual Slides: www.diagnosticpathology.eu/vs/2016_2_104/

Background

Metastasis and concomitant therapy resistance is the cause of a majority of cancer related deaths [1]. Epigenetic tumour heterogeneity is fuelled by microenvironmental factors that induce phenotypic plasticity related to epithelial-mesenchymal transition (EMT) in many tumour types [2]. In epithelial tumours, EMT is associated with a characteristic loss of normal cell polarity and adherent junctions, acquisition of fibroblastic morphology, decreased E-cadherin and gain of N-cadherin, and increased vimentin expression [3]. The EMT program is activated by dedicated transcription regulators of the Snail, Twist and Zeb families [4]. Recent evidence has shown that Axl receptor tyrosine kinase signal transduction regulates tumour EMT, malignant progression and therapy resistance [5, 6].

Axl is a member of the Tyro3, Axl, Mertk (TAM) receptor tyrosine kinases family, which share the vitamin K-dependent ligands growth arrest specific 6 (Gas6) and Protein S, although Axl responds exclusively to Gas6 [7, 8]. Axl was originally discovered as a transforming gene in chronic myeloid leukaemia [9], and has been associated with poor outcome in a wide variety of cancers including breast [5], lung [10], glioblastoma multiforme [11], prostate [12], oesophageal [7], pancreatic [13], colon [14], hepatocellular [15], ovarian [16] and acute myeloid leukaemia [17]. Furthermore, Axl expression has been associated with broad resistance to targeted therapeutics in several malignancies including non-small cell lung cancer, head and neck squamous cell carcinoma, gastrointestinal stromal tumours and melanoma [18, 19]. Thus, Axl inhibition is an attractive target for anti-cancer therapeutic development [6]. The first selective Axl inhibitor (small molecule inhibitor BGB324, formerly known as R428) is currently in Phase I clinical trials [20, 21].

To study the clinical significance of Axl expression as well as the therapeutic efficacy of Axl inhibitors such as BGB324, good diagnostic reagents in order to measure human Axl protein levels in clinical samples are critical. Therefore, we sought to develop sensitive assays for detection of Axl protein. These assays are required to reliably measure total Axl levels in patient-derived materials such as tumour tissues and blood samples and for future patient stratification according to Axl expression. Additionally, they may be useful for monitoring pharmacodynamic responses to Axl-targeting therapeutics.

We generated a panel of MAbs directed against the extracellular domains of human Axl and screened them to identify antibodies with desirable properties for ELISA, Western blot analysis and immunohistochemistry.

the diagnostic pathology journal DIAGNOSTIC PATHOLOGY

Lavina Ahmed et al, diagnostic pathology 2016, 2:104
ISSN 2364-4893
DOI: http://dx.doi.org/10.17629/www.diagnosticpathology.eu-2016-2:104

Methods

Antibodies and reagents

The mouse hybridomas producing monoclonal antibodies against human Axl receptor were generated by Biotem (Apprieu, France). Recombinant human antigens rhAxl-Fc chimera (154-AL-100), rhGas6 (885-GS-050), rhMertk-Fc chimera (891-MR-100), rhTyro3-Fc chimera (859-DK-100), recombinant mouse antigens rmAxl-Fc chimera (854-AX-100), rmGas6 (986-GS-025), and monoclonal and polyclonal anti-Axl antibodies (MAB154, AF154) were purchased from R&D Systems. Anti-glyceraldehyde 3-phosphate dehydrogenase (GAPDH) was from Invitrogen (A21994). Secondary antibodies were rabbit anti-goat IgG (H+L) (Southern Biotech, 6164-01), affinity purified goat anti-human HRP conjugate (Jackson ImmunoResearch Laboratories Inc, 109-035-098), donkey anti-goat IgG (H+L) HRP (Santa Cruz, sc-2020) and goat anti-mouse IgG (H+L) HRP (Invitrogen, G21040).

Antibody purification was performed using Protein G HP SpinTrap columns (GE Healthcare, 17-1128-01) following the manufacturer's protocol. HRP-conjugation was performed using the Lightning-Link® horseradish peroxidase kit (Innova Biosciences, 701) according to the manufacturer's instructions.

Cell-lines and culture conditions

The following human cell lines used in this study were obtained from the American Type Culture Collection: MCF 10A (CRL-10317), MDA-MB-231 (HTB-26) (triple-negative breast cancer), A549 (CCL-185) and NCI-H1299 (CRL5803) (non-small cell lung cancer), PC3 (CRL-1435) and LNCaP (CRL-1740) (prostate cancer), SKOV3 (HTB-77) (ovarian cancer), MIA PaCa-2 (CRL-1420) (pancreatic carcinoma). Melanoma cell lines WM35, and WM278 were generous gifts from Dr Ingeborg M. Bachmann. A derivative of the MDA-MB-231 cell line carrying the red fluorescent protein (RFP)-marked retroviral short hairpin ribonucleic acid (shRNA) knockdown construct shAxl2 was selected to >90% purity (judged by percent RFP-positive cells) by puromycin selection [5]. MCF10A cells expressing Axl were generated by transduction with a retroviral construct carrying full length human Axl. MDA-MB-231 and PC3 cells were cultured in complete F12 Ham's media, while the A459 and MIA PaCa-2 cells were cultured in complete DMEM media. The cell lines LNCaP, NCI-H1299, SKOV3, WM35 and WM278 were cultured in complete RPMI media. All media were supplemented with 10% foetal bovine serum, 1% pen/strep solution (100 µg/mL penicillin and 100 µg/mL streptomycin) and 1% glutamate (all purchased from Sigma-Aldrich). Depending on the cell line and in accordance with manufacturer's recommendations, supplements or additional additives, such as sodium pyruvate (A549, MIA PaCa-2 and LNCaP cells), horse serum (MIA PaCa-2) and gentamycin (A549) were added to the media. All cells were cultured at 37 ºC in humidified atmosphere with 5% CO_2.

Lavina Ahmed et al, diagnostic pathology 2016, 2:104
ISSN 2364-4893
DOI: http://dx.doi.org/10.17629/www.diagnosticpathology.eu-2016-2:104

Protein extraction and quantification

As previously described [22] cells were seeded in 10 cm dishes (Nunc, 734-2043) and grown to 95% confluence, washed with phosphate buffered saline (PBS) (Sigma-Aldrich, P4417) and lysed with RIPA lysis buffer (Thermo Scientific, 89901) with added cOmplete protease inhibitor cocktail (Roche, 0589297001), PhosSTOP phosphatase inhibitor cocktail (Roche, 04904845001), 1 mM Pefabloc (76307), 1 mM PMSF (phenyl methane sulfonyl fluoride) (P7626), 1 mM sodium vanadate (S6508) and 1 mM sodium fluoride (30105), all from Sigma-Aldrich. The cell lysates were clarified by centrifugation at 15000 *g* for 10 min and the protein content in the supernatants was determined using the BCA protein assay kit (Thermo Scientific, 23227). All protein samples were stored at −20 ºC for further use.

Sandwich ELISA

Maxisorp C 96-well microplates (Thermo Scientific, 430341) were coated overnight at 4 °C with capture antibodies at a concentration of 4µg/mL in 0.1 M sodium carbonate/bicarbonate buffer (pH 9.4). The plates were washed three times with PBS and blocked with 5% skimmed milk in PBS overnight at 4 ºC. After three more PBS washes, the plates were incubated with antigen for 2 h at RT. After a further three washes with PBS, the plates were incubated with the appropriate HRP–conjugated secondary antibody (0.3 µg/mL in 5% skimmed milk/PBS), for 1 h at RT. After a final three washes with PBS the plates were developed using tetramethylbenzidine substrate (Sigma- Aldrich, T-2885) in 100 mM sodium acetate pH 6.0), and 0.1% H_2O_2. The reaction was stopped with 1M sulphuric acid and the absorbance at 450 nm was read in a Clariostar plate reader (BMG Labtech, Ortenburg, Germany). Absorbance at a reference wavelength (595 nm) was subtracted.

SPR analysis

All binding experiments using SPR were performed using a Biacore 3000 instrument (GE Healthcare, Little Chalfont, UK) at 25 °C. Recombinant Fc chimeras (rhAxl-Fc, rhMertk-Fc or rhTyro3-Fc) were immobilized on the surfaces of a CM5 sensor chip using amine coupling at a surface density of 393.0, 303.6 and 364.0 resonance units (RU), respectively. In another set of experiments, rhAxl-Fc and rmAxl-Fc were immobilized on the surfaces of a CM5 sensor chip at a surface density of 1,308.0 and 2,115.9 RU, respectively. Blank reference surfaces were generated in parallel, without addition of antigen. The Biacore runs were performed in an automatic mode using the Binding analysis wizard (Biacore, GE Healthcare). Samples containing either MAb 1H12 or rmGas6 at concentration 10 µg/mL in HBS-EP buffer (GE Healthcare) were injected over the surfaces with immobilized antigens at flow rate of 30 µL/min for 3 min (association) followed by 5 min dissociation.

For the competitive binding study, several cycles of two-sample injection were performed using a CM5 sensor chip coated with rhAxl-Fc at surface density of 393.0 RU. As a first sample, a saturating concentration of either MAb 1H12 (1.8 µM) or MAb 5F11 (670 nM) was injected

Lavina Ahmed et al, diagnostic pathology 2016, 2:104
ISSN 2364-4893
DOI: http://dx.doi.org/10.17629/www.diagnosticpathology.eu-2016-2:104

over the surface for 3 min at flow rate of 30 µL/min followed by 2.5 min stabilization (HBS-EP buffer alone) before the injection of the following second samples: rhGas6, rmGas6, 1H12 and 5F11, all at concentration 25 µg/mL. The second sample was injected for 3 min, followed by 2.5 min stabilization (HBS-EP buffer alone) and regeneration of the surface by 30 sec injection of a regeneration solution (10 mM HCl, 1 M NaCl) at flow rate 50 µL/min.

To determine the affinity of anti-Axl antibodies 1H12 and 5F11, a CM5 sensor chip coated with rhAxl-Fc at density 190.0 RU was used. For the kinetics measurements, different concentrations of MAbs 1H12 (from 1.3 to 667 nM) and 5F11 (from 0.06 to 30 nM) in HBS-EP buffer were injected at flow rate of 30 µL/min with 3 min injection time followed by 5 min dissociation (buffer alone). After each cycle, the surface was regenerated by 30 sec injection of regeneration solution as described above. Mass transfer control experiments demonstrated absence of significant mass transfer limitations. An additional linked reaction control experiment was performed by analysing the dissociation phases after injection of antibody at a concentration of either 1.8 µM or 30 nM for MAbs 1H12 or 5F11, respectively, for 1, 3 or 20 min. The kinetic association (on-rate, k_{on}) and dissociation (off-rate, k_{off}) rates were calculated using BIAevaluation software (Biacore) and 1:1 Langmuir binding model. The equilibrium dissociation constant (K_D) was calculated as the k_{off}/k_{on} ratio. The half-life ($t_{1/2}$) of the formed antibody-antigen complexes was calculated as the $\ln 2/k_{off}$ ratio.

Western Blot analysis

For each protein sample, 10 µg total protein were separated by SDS-PAGE 4-12% gradient gel, (Thermo Scientific, NP0322BOX) and blotted onto PVDF membrane (GE Healthcare Life Sciences, 10600023). The membranes were blocked with 5% skimmed milk in Tris-buffered saline/Tween-20 (TBS-T; 25 mM Tris-HCl, 1 mM NaCl, 0.1% Tween-20) followed by overnight incubation with Axl primary antibodies at a concentration of 1 µg/mL. Loading control was detected by anti-GAPDH at 1:3000 dilution. HRP-conjugated secondary antibodies were used at 1:3000 dilution. Detection was performed using 255 mM luminol (5-amino-2, 3-dihydro-1, 4-phathalazinedione, A8511) and 90 mM enhancer (p-COUMARIC acid, C9008) in 0.1M Tris-HCl (pH 8.5) and 30% hydrogen peroxide (H_2O_2) (all from Sigma-Aldrich) and bands were imaged using a ChemiDoc™ XRS+ imager with Image lab software (BIO-RAD Hercules, CA). Bands were quantified using Image J software, normalised to the GAPDH loading control and expressed as Relative Density units [23].

Cell pellet preparation

Formalin-fixed and paraffin-embedded cell pellets were prepared as previously described [22]. Briefly, cells were cultured in T175 flasks up to 95% confluence (1×10^7 cells), trypsinized with 0.25% trypsin/ethylenediaminetetraacetic acid (Sigma-Aldrich, T4049), and collected by centrifugation at 1000 *g* for 5 min at room temperature (RT). The resulting cell pellets were transferred into clean 1.5 mL tubes and washed with PBS. Following this, 60 µL bovine plasma (Sigma-Aldrich, P4639) were added, followed by addition of 40 µl thrombin (Millipore, 604980)

Lavina Ahmed et al, diagnostic pathology 2016, 2:104
ISSN 2364-4893
DOI: http://dx.doi.org/10.17629/www.diagnosticpathology.eu-2016-2:104

to stabilise the pellets. Finally, the pellets were held in 4% formaldehyde solution overnight and transferred to 70% ethanol, prior to embedding in paraffin wax for IHC staining. Additional cell pellets were prepared from cell lines WM115, WM278, A549 and MIA PaCa2, which were fixed in 4% formaldehyde solution for 12h, 24h, 48h, 5days, 7 days and 14 days prior ethanol preservation and embedding.

Tissue microarrays

Tissue microarrays (TMA) were prepared from cell blocks or archival tissue blocks using a semi-automatic Minicore machine (Tissue Array Minicore 3, Alphelys, Plaisir, France); one (cell blocks) or 3 (archival blocks) tissue core(s) per sample at 1 mm diameter were punched out of each donor block and placed into a recipient paraffin block [24, 25].

Patient cases and paraffin embedded tissues

A variety of archival patient tissues from Norway (Department of Pathology, Haukeland University Hospital, Bergen) were used and initially screened as sample cases for this study. Briefly, these samples included lung cancer (n=21; adenocarcinoma=10, squamous cell carcinoma=11), breast (n=8; invasive carcinoma=7, DCIS=1), brain (n=5; glioblastoma=4, normal=1), malignant melanoma (n=3), thyroid (colloid goitre, n=1), kidney (n=6; carcinoma=4, normal=2), prostate (n=13; benign=6, carcinoma=7), ovary (carcinoma=1; normal=2), endometrium (n=1), tonsils (n=2), oral carcinoma (n=1), stomach carcinoma (n=1), colon carcinoma (n=5) and hepatobiliary (n=3; liver=2, bile duct=1) (**Table 4**). For half of the lung cases (n=10), corresponding preoperative percutaneous core needle biopsies were included for comparison. Regarding the lung series, sample cases from the period 2008-2012 were included. Histological re-examination of all the cases included was carried out. The Regional Committee for Medical and Health Research Ethics (REC) of Western Norway (ID# 2014/1984/REK Vest) approved this study.

Sections from primary tumours and metastases from an orthotopic xenograft of MDA-MB-231 cells in NOD.Cg-*Prkdc*^{scid} *Il2rg*^{tm1Wjl}/SzJ mice were a gift from Dr. Gro Gausdal, BerGenBio AS.

Immunohistochemical staining of formalin-fixed paraffin-embedded sections

Paraffin blocks of cell pellets (n=10); xenograft tumour sections (n=2) and archival patient samples, (n=78) were sectioned at 5µm and mounted onto glass slides and deparaffinised in xylene, rehydrated through a series of decreasing concentrations of alcohol and rinsed in distilled water. Antigen retrieval using target retrieval buffer pH6 (Dako, S1699) was achieved by heating the slides in either a microwave (6th Sense Jetchef Microwave Oven JT 366, Whirlpool, Benton Harbor, MI) (25 min, cell pellets; 30 min, xenograft tumour tissue) or a pressure cooker (archival patient samples). Briefly, sections were heated in the pressure chamber (Decloaking Chamber^{TM} Plus; Model: DC2008INTL; Biocare Medical, Concord, CA) at 125 °C ± 5 °C at 17-24 psi, maintained for 35 s. The time taken to reach the temperature

Lavina Ahmed et al, diagnostic pathology 2016, 2:104
ISSN 2364-4893
DOI: http://dx.doi.org/10.17629/www.diagnosticpathology.eu-2016-2:104

averaged around 15 min. Sections were allowed to cool within the chamber. Cooling from 90 °C to 75 °C was assisted by a fan within the cooker. Following antigen retrieval, the slides were allowed to cool to RT for 20 min and rinsed with Dako wash buffer solution (S3306). Subsequently, the slides were incubated for 1 h at RT with MAb 1H12 (1 µg/mL), which was either preceded (cell pellets and xenograft samples) or followed (archival patient samples) by endogenous peroxidase blocking with 0.03% peroxidase block (S2001) for 8 min, followed by rinsing with distilled water and incubation in wash buffer solution for 5 min. Alternatively, the cell pellet sections from parental and Axl-knocked down MDA-MB-231 cells were incubated with AF154 (0.031 µg/mL, overnight at 4 ºC) or MAB154 (1 µg/mL for 1 h at RT). The AF154-stained slides were further incubated with rabbit anti-goat IgG (H+L) secondary antibody (Southern Biotech, 6164-01) diluted 1:400 for 30 min at RT.

For the 1H12 stained archival tissue sections, the HiDef antigen detection HRP-polymer anti-mouse system (Cell Marque, 954D-4030) was applied for a total of 20 min to visualize the bound antigen. EnVision+System-HRP/labeled polymer anti-mouse (Dako, K4065) was used for MAb 1H12 and MAB154 stained cell pellets, while the anti-rabbit (Dako, K4011) was employed for AF154 stained sections, both for 30 min at RT. The HiDef antigen detection HRP polymer system is a two-step system that includes application of an amplifier for 10 min followed, after rinsing with buffer, by the HRP reagent for 10 min. The peroxidase was developed by incubation with freshly prepared 3, 3'-diaminobenzidine chromogen solution (Dako, K3468) for 5-10 min and rinsed with distilled water. The sections were counterstained with haematoxylin (Dako, S2020).

Evaluation of 1H12 staining

For the archival TMA and the cell pellet sections, the strength of staining was determined subjectively by microscopy as: 0 (negative), 1+ (mild/weak), 2+ (moderate), 3+ (strong). The staining was considered positive when it was stronger than any background staining present. Regarding the lung cases, evaluation was done using a staining index (SI) with values from 0 to 9, which was obtained by multiplying the score for intensity of staining (as above) with the score for proportion of tumour cells stained (1, <10%; 2, 10-50%; 3, >50%) [26]. Based on the median SI, the cut-off points were set as negative (0-1) or positive (2-9).

Normal human tissue reactivity study using IHC on cryosections

A normal human tissue reactivity study of MAb 1H12 was performed by MicroMorph Histology Services (Lund, Sweden) using commercial frozen TMA purchased from BioChain (T6234701-2). Frozen pellets of Axl^+ and Axl^- cells were used as positive and negative controls and to determine optimal antibody concentration. MAb 1H12 showed moderate to strong reaction in the Axl^+ cells from 8 down to 1 µg/mL; at 0.5 µg/mL the reaction was moderate. The optimal concentration of 1 µg/mL was therefore used. At this concentration, no reaction was seen in the Axl^- cells.

the diagnostic pathology journal DIAGNOSTIC PATHOLOGY

Lavina Ahmed et al, diagnostic pathology 2016, 2:104
ISSN 2364-4893
DOI: http://dx.doi.org/10.17629/www.diagnosticpathology.eu-2016-2:104

Acetone fixed cryosections at 8 µm were blocked in 5% normal goat serum (Jackson ImmunoResearch, 005-000-121) for 30 min. The sections were then stained with primary antibody (1H12) in PBS with 5% goat normal serum for 1 h, and washed three times in PBS. Subsequently, the sections were stained with EnVision mouse (Dako, K4001) for 30 min. Finally, the sections were washed three times in Tris buffer, before they were stained with 3, 3'-diaminobenzidine chromogen for 5 min. Staining intensity was judged as: negative (0), weak reaction (1+), moderate reaction (2+), or strong reaction (3+).

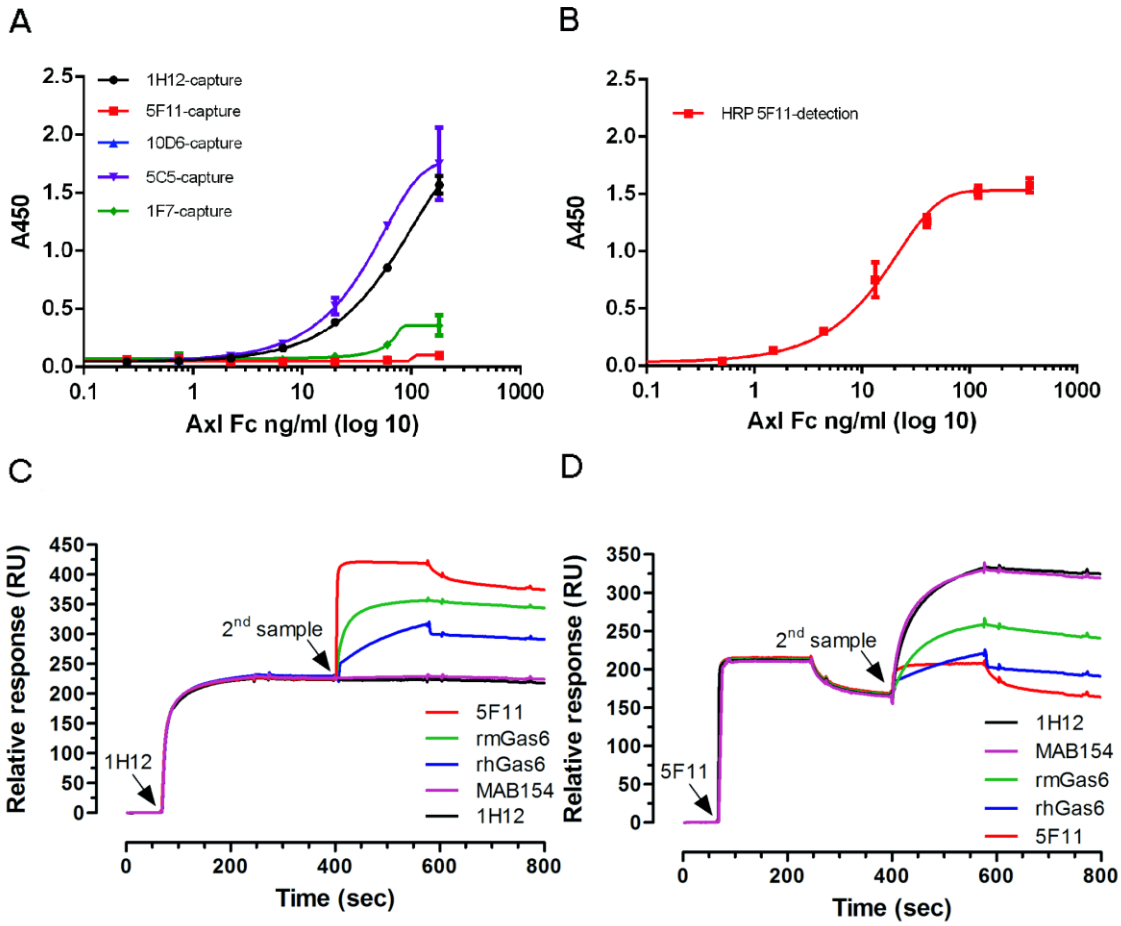

Figure 1: (A) Representative sandwich ELISA using MAb 1H12 as capture Ab, Axl-Fc as antigen and comparing 5F11, 10D6, 5C5 and 1F7 as detection antibodies. **(B)** Representative titration curve of Axl-Fc using 1H12 as capture antibody and HRP-5F11 for detection. Mean ± SD is shown for both. **(C, D)** Biacore 3000 sensorgrams of binding to immobilised Axl-Fc. Initial binding of MAb 1H12 **(C)** or MAb 5F11 **(D)** does not interfere with subsequent binding (indicated as 2nd sample) of the other antibody, rhGas6 or rmGas6. Arrows indicate injections of analytes.

Lavina Ahmed et al, diagnostic pathology 2016, 2:104
ISSN 2364-4893
DOI: http://dx.doi.org/10.17629/www.diagnosticpathology.eu-2016-2:104

Results

Monoclonal antibody generation

Three female OF1 mice were immunized over 10 days with rhAxl-Fc, a recombinant antigen comprising the extracellular domains of human Axl fused to the human IgG1 Fc portion. Initial hybridoma colonies were screened by ELISA against immobilized rhAxl-Fc, and by cellular ELISA against a cell line expressing Axl (MCF-10A-Axl) and a control cell line not expressing Axl (MCF-10A) [5]. Cells from 62 positive oligo/monoclonal wells were cryopreserved, and antibodies from the culture supernatants were isotyped and further characterized by flow cytometry using Axl-positive MDA-MB-231 cells compared to Axl-negative MDA-MB-231shAxl2 cells expressing an Axl knockdown shRNA construct [5]. Antibodies demonstrating binding to Axl by flow cytometry were purified over Protein G columns. Thirty antibodies were excluded on the basis of isotype (IgM, 8 Abs), poor or negative staining of Axl positive cells by flow cytometry (16 Abs) or poor yield from Protein G purification (< 50 ng/mL, 6 Abs). This left a panel of 32 anti-Axl antibodies for further characterization.

Table 1: Summary of sandwich ELISA results of compatible antibody pairs

Capture Antibodies	**Detection Antibodies**				
	HRP-1H12	HRP-5F11	HRP-10D6	HRP-5C5	HRP-1F7
1H12	–	+	+	+	+
5F11	+	–	–	+	–
10D6	+	–	–	+	–
5C5	+	+	+	–	+
1F7	+	–	–	+	–

Sandwich-ELISA was performed using all 25 combinations of capture and detection antibodies. (+) denotes compatibility between capture and detection antibodies and (−) that the pairs were not compatible.

the diagnostic pathology journal DIAGNOSTIC PATHOLOGY

Lavina Ahmed et al, diagnostic pathology 2016, 2:104
ISSN 2364-4893
DOI: http://dx.doi.org/10.17629/www.diagnosticpathology.eu-2016-2:104

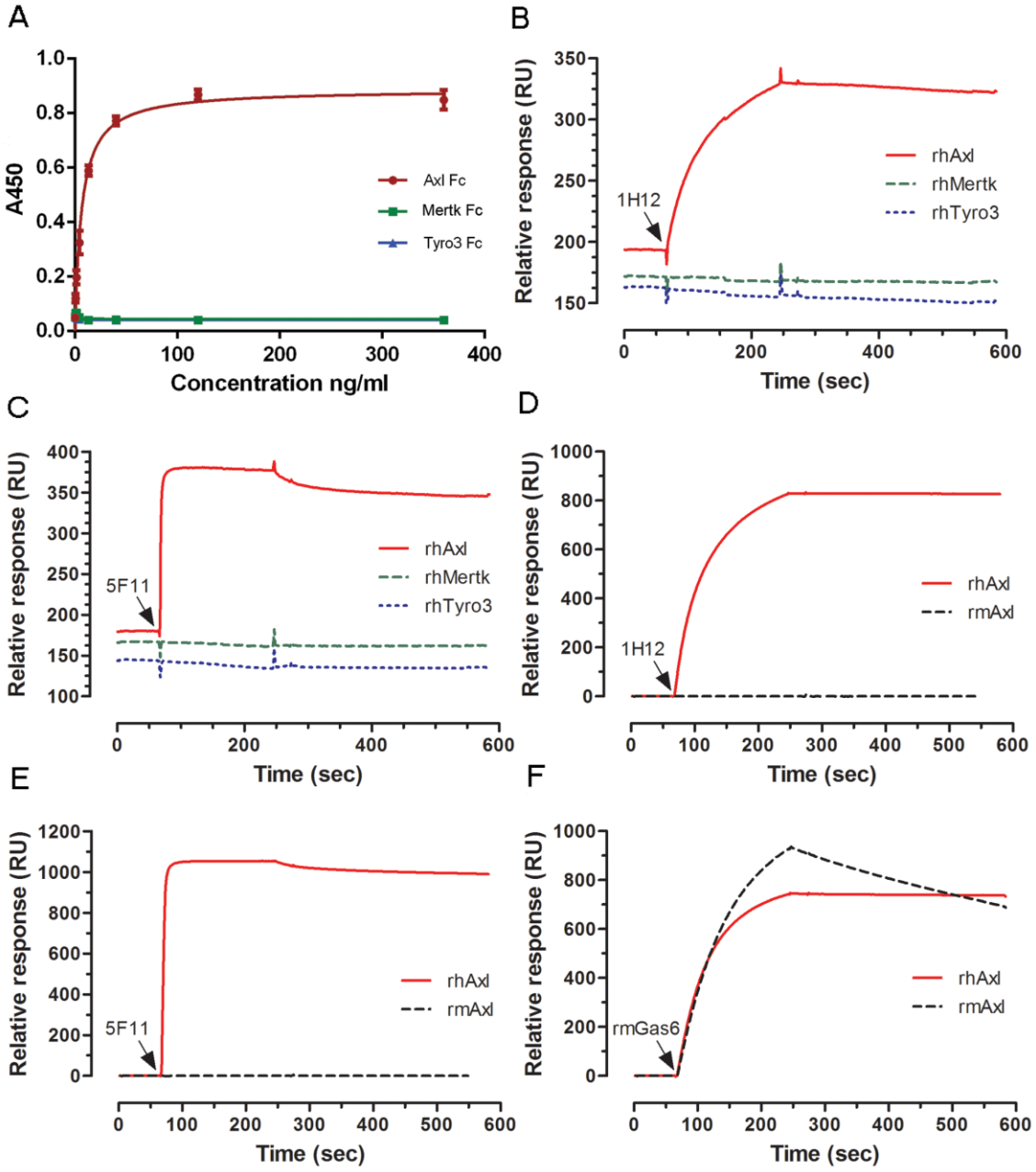

Figure 2: Analysis of 1H12 and 5F11 specificity. (**A**) MAb 1H12 binding recombinant human TAM receptors (Tyro3, Axl or Mertk fused to human Fc) in ELISA. Detection of bound Fc chimeras was performed using goat anti-human HRP conjugate. (**B, C**) Biacore 3000 sensorgrams of MAbs 1H12 and 5F11 binding to immobilised recombinant human TAM receptor-Fc chimeras. (**D**-**F**) Biacore 3000 sensorgrams of MAb 1H12 (**D**), 5F11 (**E**) or rmGas6 (**F**) binding to immobilized rhAxl-Fc or rmAxl-Fc. Sensorgrams are shown after subtraction of signals from a blank surface. Arrows indicate injections of analytes, MAb 1H12, 5F11 or rmGas6.

Lavina Ahmed et al, diagnostic pathology 2016, 2:104
ISSN 2364-4893
DOI: http://dx.doi.org/10.17629/www.diagnosticpathology.eu-2016-2:104

Selection of antibodies for sandwich-ELISA

The panel of 32 mouse antibodies were characterized at equal concentrations by SPR (Biacore) analysis against immobilized Axl-Fc. Ten were excluded on the basis of poor or undetectable binding, or high off-rate. The remaining 22 antibodies were screened as capture antibodies for ELISA, using Axl-Fc as the antigen and an HRP-anti-human Ig secondary for detection. Five candidates (1H12, 5F11, 10D6, 5C5 and 1F7) were selected for further characterization based on signal-to-noise ratio. The parent hybridomas were thawed and subject to one (10D6, 5F11) or two (1H12, 5C5, 1F7) further rounds of subcloning to generate pure monoclonal populations. For further characterization, the antibodies were then purified from approximately 15 mL of hybridoma culture supernatant by Protein G affinity chromatography. Antibody-HRP conjugates of each antibody were prepared and all twenty-five possible combinations of unconjugated capture antibody versus conjugated detection antibody were tested for compatibility (**Table 1** and **Fig. 1A**). From **Table 1** we concluded that antibodies 5F11, 10D6 and 1F7 recognise epitopes that are too close together to allow simultaneous recognition but that 1H12 and 5C5 were compatible with each of the other antibodies. Checkerboard titration using 0.5, 1, 2, or 4 µg/mL of 1H12 or 5C5 as capture antibody versus 0.05, 0.1, 0.3 and 0.6 µg/mL of each detection antibody and 0 ng/mL or 2 ng/mL of Axl-Fc antigen was performed to find conditions with the best signal-to-noise ratio for low antigen concentrations. MAb 1H12 gave generally higher signal-to-noise ratios than 5C5 and was, therefore, selected as the capture antibody. The combination of 1H12 coated at 4 µg/mL and the antibodies HRP-5F11 or HRP-10D6 at 0.3 µg/mL gave the best ratios (approximately 6); HRP-5F11 was selected as the detection antibody. A representative titration curve using the mentioned conditions is shown in **Figure 1B** and suggests that the Axl detection limit is as low as 2 ng/mL.

The binding of MAbs 1H12 and 5F11 to Axl-Fc was further characterised by competitive binding using SPR measurements. The results confirmed that these two antibodies bind independently to Axl-Fc, and that neither 1H12 nor 5F11 interferes with Axl binding to its ligand Gas6 (**Fig. 1C** and **D**).

Characterisation of specificity and selectivity of 1H12 and 5F11

The specificity of the antibodies 1H12 and 5F11 for detection of human Axl was analysed using both sandwich-ELISA and SPR measurements. **Figure 2A-C** demonstrates that antibodies 1H12 and 5F11 specifically recognized human Axl and did not show any binding to the other TAM receptor family members, Mertk and Tyro3. Furthermore, the MAbs 1H12 and 5F11 showed no cross-reactivity with mouse Axl (**Fig. 2D and E**). Recombinant mouse Gas6 (rmGas6), the ligand for Axl, was used as a positive control to demonstrate the presence of intact protein on the SPR sensor surface (**Fig. 2F**).

the diagnostic pathology journal DIAGNOSTIC PATHOLOGY

Lavina Ahmed et al, diagnostic pathology 2016, 2:104
ISSN 2364-4893
DOI: http://dx.doi.org/10.17629/www.diagnosticpathology.eu-2016-2:104

Table 2: Affinity constants of MAb 1H12 and 5F11 for binding to human Axl.

MAb	On-rate (k_{on}; $M^{-1}s^{-1}$)	Off-rate (k_{off}; s^{-1})	K_D (M)	Half-life ($t_{1/2}$; h)
1H12	2.14×10^{5}	1.07×10^{-5}	4.98×10^{-11}	18.0
5F11	2.15×10^{7}	1.25×10^{-4}	5.80×10^{-12}	1.5

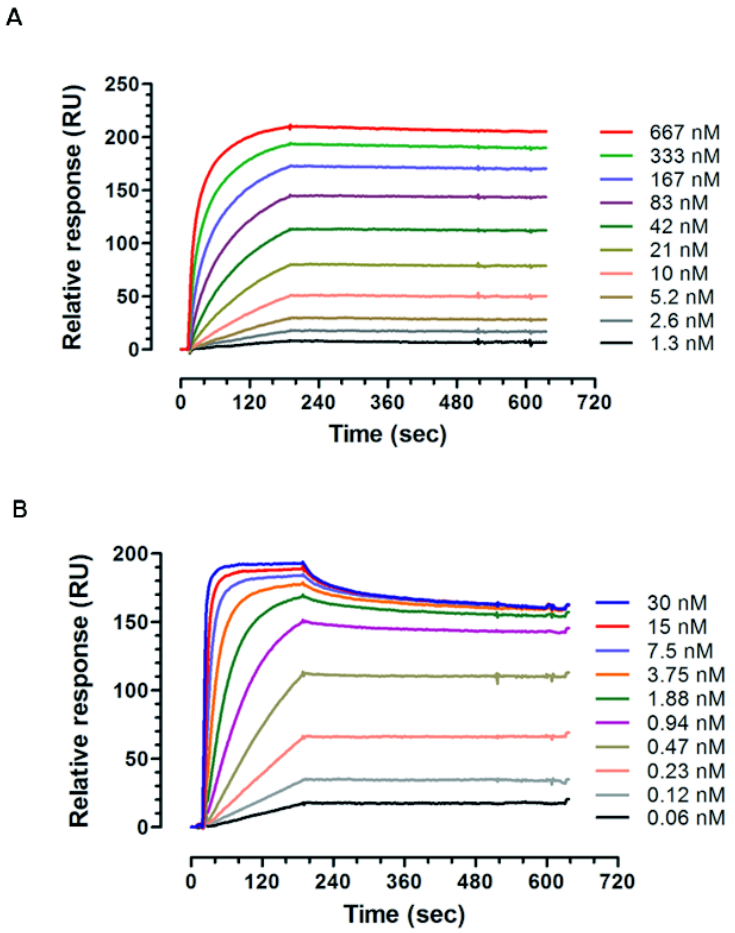

Figure 3: Kinetic analysis of MAbs 1H12 (**A**) and 5F11 (**B**) interacting with rhAxl immobilized on the surface of the Biacore sensor chip. Overlay plots of sensorgrams for different concentrations of MAb 1H12 (1.3 – 667 nM) and MAb 5F11 (0.06 – 30 nM) are shown in panels **A** and **B**, respectively. The affinity constants (kinetic and steady state) as well as the calculated half-live of antigen binding at 25 °C are shown in **Table 2**.

Lavina Ahmed et al, diagnostic pathology 2016, 2:104
ISSN 2364-4893
DOI: http://dx.doi.org/10.17629/www.diagnosticpathology.eu-2016-2:104

Figure 3 and **Table 2** show that the mouse MAb 1H12 demonstrated very high affinity of binding to human Axl with a K_D value of 49.8 pM, mainly due to a very slow dissociation rate (k_{off} = 1.07 × 10^{-5} 1/s^{-1}) that resulted in an 18 h half-life for the 1H12/Axl complex. Even higher affinity (5.8 pM) was demonstrated by the antibody 5F11 (**Table 2**), however, due to extremely fast on-rate of Axl binding (k_{on} = 2.15 × 10^7 1/$M^{-1}s^{-1}$). Taken together, both 1H12 and 5F11 are high-affinity MAbs highly specific for detection of human Axl in a given sample.

Selection of antibodies for immunohistochemistry

All the 32 MAbs were screened at identical concentration against formalin-fixed and paraffin-embedded (FFPE) sections of cell pellets of either Axl^+ MDA-MB-231 cells or Axl^- MDA-MB-231shAxl2 cells. Among all the tested antibodies, MAb 1H12 gave the strongest membrane staining with minimal nuclear or cytoplasmic background. The best staining of Axl^+ cells with MAb 1H12 was achieved with a concentration of 1 µg/mL (high-score positive staining of cell membranes and weak or no cytoplasmic staining), while the Axl^- cells showed predominantly negative staining with some weak expression in scattered single cells (**Fig. 4A**). The presence of isolated Axl-expressing cells was consistent with the observed purity of the MDA-MB-231shAxl2, since the flow cytometry results indicated that approximately 90% of the cells carried the retroviral shRNA construct (data not shown).

Comparison of antibodies in immunohistochemistry and Western blot analysis

We compared the staining observed with 1H12 (1 µg/mL) to that seen using the commercially available antibodies AF154 (polyclonal) and MAB154 (monoclonal). At an optimized dilution of 1: 6400 (0.03 µg/mL), AF154 demonstrated fairly strong membrane staining with some expression also observed in scattered Axl^- cells. However, some weaker cytoplasmic background staining was observed in a majority of the cells (**Fig. 4A**). Staining with monoclonal antibody MAB154 at 1µg/mL demonstrated slightly weaker signal than with MAb 1H12 on Axl^+ cells at the same concentrations, although staining with MAB154 was still well defined in the cell membrane. The staining pattern seen with 1H12 is therefore consistent with the staining pattern of existing antibodies.

Similar comparisons were done by Western blot analysis of Axl^+ and Axl^- cell lysates using MAb 1H12, AF154 and MAB154 (**Fig. 4B**). All three antibodies were used at concentration of 1 µg/mL for the purpose of comparison. All antibodies detected a distinct protein band with an apparent molecular weight of approximately 140 kDa present in the Axl^+ cell lysate but not in the Axl^- lysate, consistent with the reported size of fully-glycosylated Axl [9]. A second, somewhat weaker, band of approximately 120kDa was also often observed, consistent with the reported size of partially glycosylated Axl. All three antibodies also detected a weaker and more diffuse band with an apparent molecular weight of approximately 80 kDa that likely represents soluble Axl, formed by proteolytic cleavage of the extracellular domains [9]. Antibody AF154 displayed some additional staining of some proteins (bands) in the Axl^- lysate that migrate close to the expected size of fully-glycosylated Axl, potentially limiting its utility in

the diagnostic pathology journal DIAGNOSTIC PATHOLOGY

Lavina Ahmed et al, diagnostic pathology 2016, 2:104
ISSN 2364-4893
DOI: http://dx.doi.org/10.17629/www.diagnosticpathology.eu-2016-2:104

Western blot applications. Background staining with MAB154 and 1H12 was generally reduced compared to AF154 with no background bands at the expected sizes of Axl protein (**Fig. 4B**).

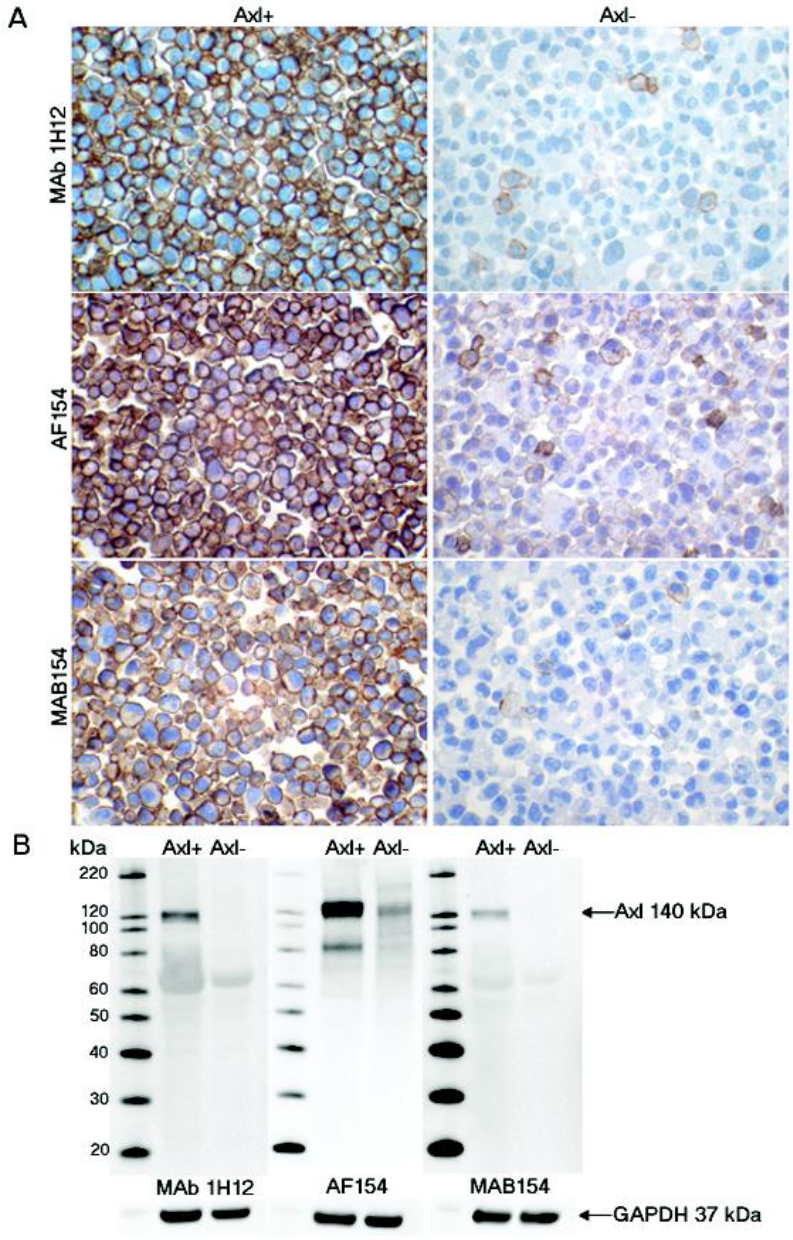

Figure 4: Comparative IHC staining of Axl^+ and Axl^- (**A**) cells using MAb 1H12, commercial antibodies polyclonal AF154 and monoclonal MAB154. Parental and Axl-knocked down MDA-MB-231 cells were used as Axl^+ and Axl^- cells, respectively. All panel show ×630 magnification. **(B)** Comparative Western blot analysis of Axl^+ and Axl^- cell lysates (parental and Axl-knocked-down MDA-MB-231 cells) developed using either MAb 1H12, polyclonal AF154 or monoclonal MAB154. As a loading control, GAPDH detection is shown on every blot.

the diagnostic pathology journal DIAGNOSTIC PATHOLOGY

Lavina Ahmed et al, diagnostic pathology 2016, 2:104
ISSN 2364-4893
DOI: http://dx.doi.org/10.17629/www.diagnosticpathology.eu-2016-2:104

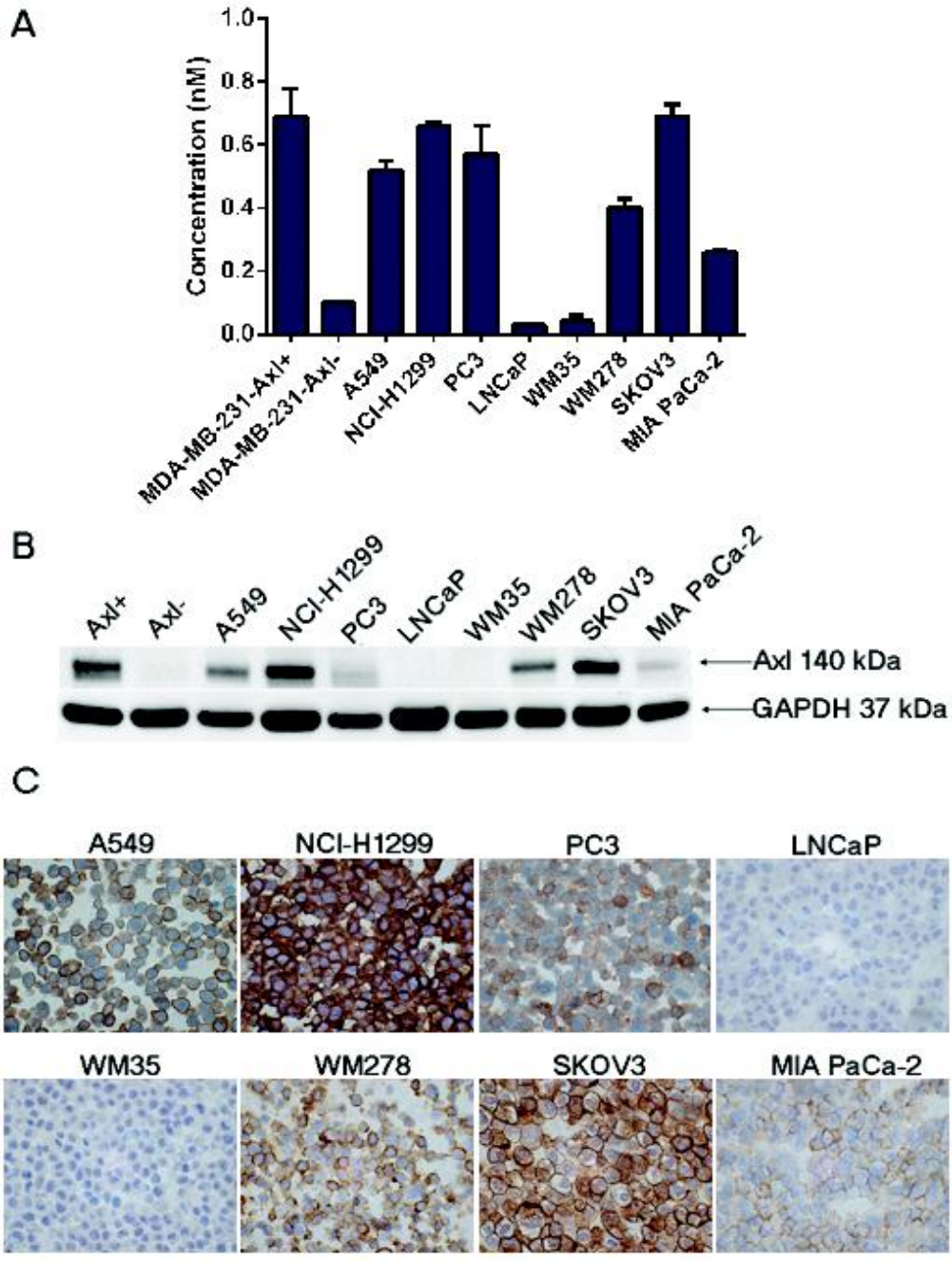

Figure 5: 1H12 correlation studies in three different assays using selection of cancer cell lines: MDA-MB-231-Axl^{+} and MDA-MB-231-Axl^{-}, breast cancer; A549 and NCI-H1299, lung; PC3 and LNCaP, prostate; WM35 and WM278, melanoma; SKOV3, ovary and MIA PaCa-2, pancreas. **(A)** Axl expression levels in a selection of cancer cell lines (approximately 2.5 × 10^6 cells/mL) in sandwich ELISA. **(B)** Western blot analysis and **(C)** Immunohistochemical staining on a panel of FFPE cell pellets derived from the cell lines. All panel show ×630 magnification.

Lavina Ahmed et al, diagnostic pathology 2016, 2:104
ISSN 2364-4893
DOI: http://dx.doi.org/10.17629/www.diagnosticpathology.eu-2016-2:104

Use of MAb 1H12 for Axl detection in different human tumour cell lines

We evaluated the performance of MAb 1H12 in three different assays – sandwich ELISA (**Fig. 5A**) Western blot analysis (**Fig. 5B**), and IHC (**Fig. 5C**) – using a panel of different human cancer cell lines. All three assays suggest moderate-to-high Axl expression in MDA-MB-231 (triple negative breast cancer), A549 and NCI-H1299 (non-small cell lung cancer), PC3 (prostate cancer), WM278 (melanoma), SKOV3 (ovarian cancer) and MIA PaCa-2 (pancreatic carcinoma) cells, with little or no expression in MDA-MB-231shAxl2, LNCaP (prostate cancer) or WM35 (melanoma) cells [27, 28].

Quantification of ELISA (using Axl-Fc standard curve), Western blots (densitometry) and IHC staining (Staining index, [SI] score) is shown in **Table 3** and compared with published gene-expression data from microarrays [27, 28]. The Pearson correlation coefficients between pairs of assays were r = 0.94 (Western blot vs. ELISA); r = 0.98 (IHC vs. ELISA); and r = 0.97 (Western blot vs. IHC) indicating that the three assays give comparable results. For those cell lines for which gene-expression data was directly comparable, there was also an excellent correspondence between the gene-expression level and the three assays (r = 0.89 – 0.98).

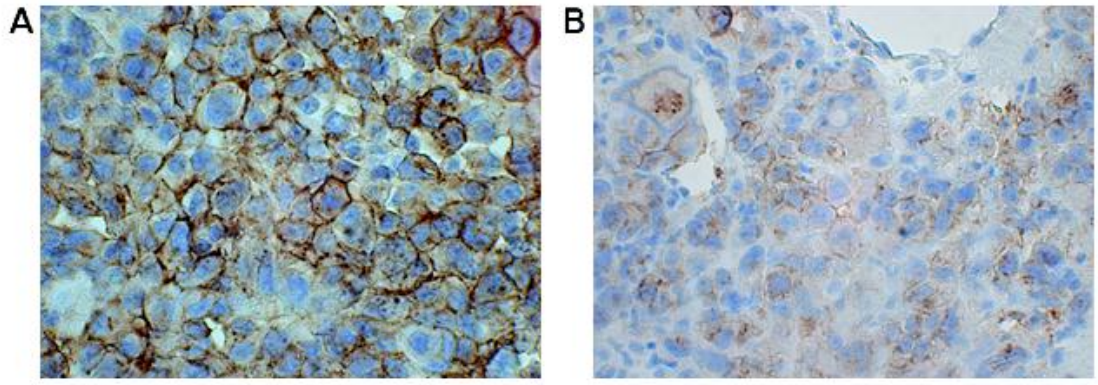

Figure 6: MAb 1H12 staining on FFPE tissue sections of xenograft tumours. **(A)** Primary breast tumour and **(B)** corresponding lung metastasis in the same mouse. Tumours were generated by orthotopic injection of MDA-MB-231 cells into the mammary fat pad of immunodeficient mice. Both panels show ×630 magnification.

Application of MAb 1H12 on tumour samples

Using IHC staining, MAb 1H12 was able to detect Axl expression in xenograft tumours collected both from the primary tumour site (**Fig. 6A**) and lung metastases (**Fig. 6B**). As expected, MAb 1H12 showed distinct membranous staining in these xenograft tumour sections, with presence of some cytoplasmic staining.

the diagnostic pathology journal DIAGNOSTIC PATHOLOGY

Lavina Ahmed et al, diagnostic pathology 2016, 2:104
ISSN 2364-4893
DOI: http://dx.doi.org/10.17629/www.diagnosticpathology.eu-2016-2:104

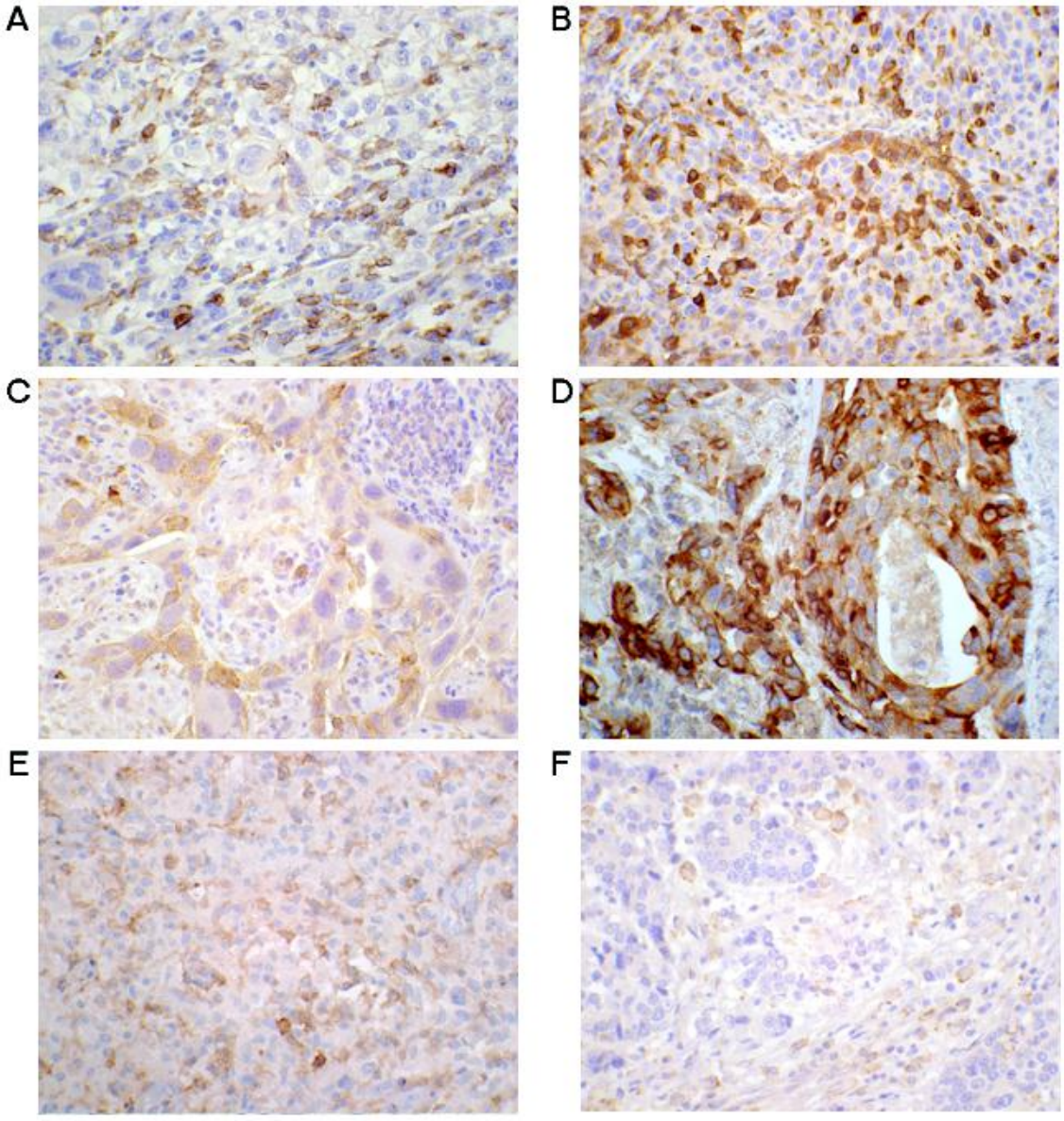

Figure 7: MAb 1H12 staining on FFPE sections from archival human tumour tissues. 1H12 staining shows moderate-to-strong membranous staining with some cytoplasmic expression in **(A)** basal-like breast cancer, **(B)** triple negative breast cancer, **(C)** lung squamous cell carcinoma, **(D)** lung adenocarcinoma, **(E)** glioblastoma and **(F)** in gastric cancer. All panels show ×400 magnification.

Staining with MAb 1H12 on sections from archival paraffin-embedded human cancers (**Table 4**) including breast carcinoma, lung adenocarcinoma and squamous cell carcinoma, and gastric carcinoma, showed distinct staining localized to the cell membrane although cytoplasmic staining was also observed in some cases (**Fig. 7**). In basal-like (**Fig. 7A**) and triple negative

Lavina Ahmed et al, diagnostic pathology 2016, 2:104
ISSN 2364-4893
DOI: http://dx.doi.org/10.17629/www.diagnosticpathology.eu-2016-2:104

breast cancers (**Fig. 7B**), strong membranous staining was observed with some weak cytoplasmic expression. In lung cancer, positive 1H12 staining was seen both in the squamous cell carcinoma (**Fig. 7C**) and in adenocarcinoma (**Fig. 7D**), with a high concordance between the staining of preoperative samples and operative lung cancer specimens (Spearman's correlation coefficient=0.76, p=0.01 for staining index comparisons). However, the staining pattern was mainly focal in squamous cell carcinoma. Moderate membranous staining in glioblastoma (**Fig. 7E**) and gastric cancer (**Fig. 7F**) was also observed.

Table 3. Quantification of Sandwich-ELISA, Western blot and IHC

Cell lines	Sandwich-ELISA (nM)	Western Blot (Relative Density)[a]	IHC (SI score)	Microarray of Gene Expression data[b]
MB-MDA-231 Axl^+	0.69	95	9	10.9
MB-MDA-231 Axl^-	0.10	4	1	Not available
A459	0.52	61	6	9.1
NCI-H1299	0.66	92	9	10.5
PC-3	0.57	37	6	9.6
LNCaP	0.03	2	0	4.9
WM35	0.04	4	0	5.2[c]
WM278	0.40	59	6	1440.0[d]
SKOV3	0.69	95	9	9.9
MIA PaCa-2	0.26	27	4	7.69

[a]Image J was used to quantify each band of Western blot analysis and percentages was obtained. Correlation coefficient between sandwich ELISA and Western blot analysis was 0.94, between sandwich ELISA and IHC was 0.98, and between Western blot and IHC was 0.97. [b]The data was compared with published gene-expression data from microarrays [27, 28]. [c,d]Gene expression data of the melanoma cell lines WM35 and WM278 was generated in a different dataset as they were not available from the cancer cell line encyclopaedia. Thus they cannot be directly compared with other cell lines.

the diagnostic pathology journal DIAGNOSTIC PATHOLOGY

Lavina Ahmed et al, diagnostic pathology 2016, 2:104
ISSN 2364-4893
DOI: http://dx.doi.org/10.17629/www.diagnosticpathology.eu-2016-2:104

In addition, strong membranous staining of alveolar macrophages (**Fig. 8A**) in lung cancers and in the lymphohistiocytic host response areas of melanoma was evident (**Fig. 8B**), as well as weak to moderate staining of endothelial cells and pericytes in both normal and tumour-associated vessels (**Fig. 8C**) in different tissues, consistent with reported expression of Axl in immune cells and the vasculature [29, 30].

A few FFPE sections from normal tissue and benign human lesions (**Table 4**) including liver (**Fig. 8D**), prostate (**Fig. 8E**), ovary (**Fig. 8F**) and kidney (**Table 4**), and cryosections of a variety of normal human tissues (**Additional file 1, Table S1**), were independently stained with MAb 1H12. Regarding the FFPE tissues, the results showed strong positive staining in the endothelial lining of the sinusoid system of the liver and in Kupffer cells [29] (**Fig. 8D**), and weak Axl expression in basal cells of prostatic glands (**Fig. 8E**) and the renal glomeruli (**Table 4**). In cryosections, most tissues showed negative or very limited Axl expression, where tissues such as lung, colon, kidney, heart, and bone marrow showed weak staining results assumed to be non-specific, while moderate to strong membranous and some cytoplasmic staining was observed in many cells of lymph nodes, spleen and some epithelial cells of the pancreas (**Additional file 1, Table S1**).We also investigated whether IHC staining with MAb 1H12 deteriorates with prolonged formalin fixation time; we used FFPE cell pellets from selected cancer cell lines. The pellets were prepared from 4 different cell lines: WM115, WM278, A549 and MIA PaCa-2 and fixed for varying periods of time ranging from 12 h to 2 weeks. The results indicate that 24-48 h fixation appear to give the best staining result in these cell line pellets (**Additional file 2, Fig S1)**.

Table 4: Observed staining of various human tissues using MAb 1H12.

Tissue (n)	**Staining pattern**	
	Strength	**Location of staining**
Normal/benign tissues		
Liver (2)	3+	Clear diffuse well-distributed staining in endothelial lining of the sinusoid system of the liver and in Kupffer cells.
Kidney (2)	2+ – 3+	Focal staining in basement membrane of the glomeruli and in some tubules; staining also seen in microvessels and in a few cells in the stroma; maybe in macrophages.
Vessels	1+ – 3+	Focal to diffuse staining of endothelial lining seen in different tissues.
Brain (1)	none	none

the diagnostic pathology journal DIAGNOSTIC PATHOLOGY

Lavina Ahmed et al, diagnostic pathology 2016, 2:104
ISSN 2364-4893
DOI: http://dx.doi.org/10.17629/www.diagnosticpathology.eu-2016-2:104

Heart (1)	none	none
Endometrium (1)	none	none
Ovary (2)	none	none
Placenta (1)	none	1+ staining seen in some of the vessels
Prostate (6) (benign)	none	Weak staining in basal cells
Thyroid (1) (goitre)	none	none
Tonsils (2)	2+ – 3+	Patchy (focal) staining of squamous epithelium. Positive staining in many of the cells in the tonsils.
Pre-cancerous lesion		
Breast (DCIS) (1)	1+	Membranous staining in a few cells.
Primary tumours		
Brain tumour (4) (Glioblastoma)	2+ – 3+	Both membranous and cytoplasmic in a few tumour cells in 3/4 cases and 1+ – 2+ specific staining of microvessels. Moderate to strong (2+ – 3+) background staining.
Breast cancer (7)	1+ – 3+	Positive epithelial cells in 2 of 7 cases, mainly membranous plus some cytoplasmic. Both focal and diffuse patterns were seen. Staining of microvessels and of the cellular infiltration in the stroma in some cases was seen.
Carcinoma of oral mucosa (1)	1+ – 2+	Positive epithelial cells; mainly cytoplasmic (1+) and some membranous (2+).
Lung cancer (10) adenocarcinoma	1+ – 3+	Positive epithelial cells in 3/10 cases; mainly membranous plus some cytoplasmic: Both focal and diffuse patterns were seen. Positive membranous staining of alveolar macrophages was seen.
Lung cancer (11) squamous cell carcinoma	1+ – 3+	Positive epithelial cells in 7/11 cases; mainly cytoplasmic plus some membranous staining. Also, moderate to strong staining seen in the dendritic-like cells between tumour cells.
Stomach cancer (1)	2+ – 3+	Membranous staining in loose cells which looked like tumour cells, in some. Weak (1+) staining in some microvessels was present.
Bile duct cancer (1)	1+	Weak (1+) staining in the cell membrane of cells in the lumen.
Colon cancer (4)	None	Tumour cells are not stained but weak (1+) staining seen in microvessels.

Lavina Ahmed et al, diagnostic pathology 2016, 2:104
ISSN 2364-4893
DOI: http://dx.doi.org/10.17629/www.diagnosticpathology.eu-2016-2:104

Ovarian cancer (1)	None	None
Prostate cancer (7)	None	Very faint barely perceptible in cells that look like basal cells.
Kidney cancer (3) (clear cell)	None	Tumour cells were unstained, but in one of the cases, both cytoplasmic and membranous 1+ - 2+ staining of stromal elements like microvessels was seen.
Malignant Melanoma (2)	None	Specific staining in the lymphohistocytic host response areas probably in the leucocyte membranes was seen
Metastatic tumours		
Metastases to liver (2)	None	Staining in stromal fibroblasts in one of the cases was seen.
Metastatic melanoma (lymph node) (1)	None	2+ – 3+ membranous staining of a number of scattered single cells, probably leucocytes, was seen.
Metastases (colon) to kidney (1)	None	None

Discussion

Biomarkers play very important roles in diagnostics and drug development [31]. Patient stratification for targeted treatment by sensitive predictive biomarkers is crucial to ensure clinical benefit, avoid over-treatment and obtain cost-effective disease management. Axl, a receptor tyrosine kinase, is overexpressed in many cancer types and correlates invariably with poor prognosis [32]. Axl regulates EMT-mediated tumour cell survival, invasiveness and drug resistance in a wide variety of cancer cell types [5, 6, 33]. Several Axl-targeting agents are in preclinical development and a clinical-stage small molecule Axl kinase inhibitor BGB324 (R428) is currently in Phase I clinical trials [20, 21]. To study whether Axl expression might be a good diagnostic biomarker for patient prognostication or as a predictor of response to Axl targeted therapy, accurate detection of Axl expression levels in patient samples with sensitive and specific detection assays is paramount.

In the present study, we describe the generation and characterization of novel MAbs against the extracellular domain of human Axl for use in different diagnostic assays for improved detection of Axl expression in patient materials. For ELISA, one of the most widely used diagnostic tools, we found that the MAb 1H12 when paired with HRP-conjugated MAb 5F11 performed well in sandwich-ELISA with high sensitivity. This pair of antibodies recognizes different epitopes, and neither antibody interferes with binding of the Axl ligand Gas6 to Axl.

Lavina Ahmed et al, diagnostic pathology 2016, 2:104
ISSN 2364-4893
DOI: http://dx.doi.org/10.17629/www.diagnosticpathology.eu-2016-2:104

Furthermore, both 1H12 and 5F11 demonstrate high affinity for human Axl (two- and one-digit picomolar range, respectively) and are also highly specific; no binding was observed to other members of the human TAM receptor family (Mertk or Tyro3), or to the murine Axl receptor.

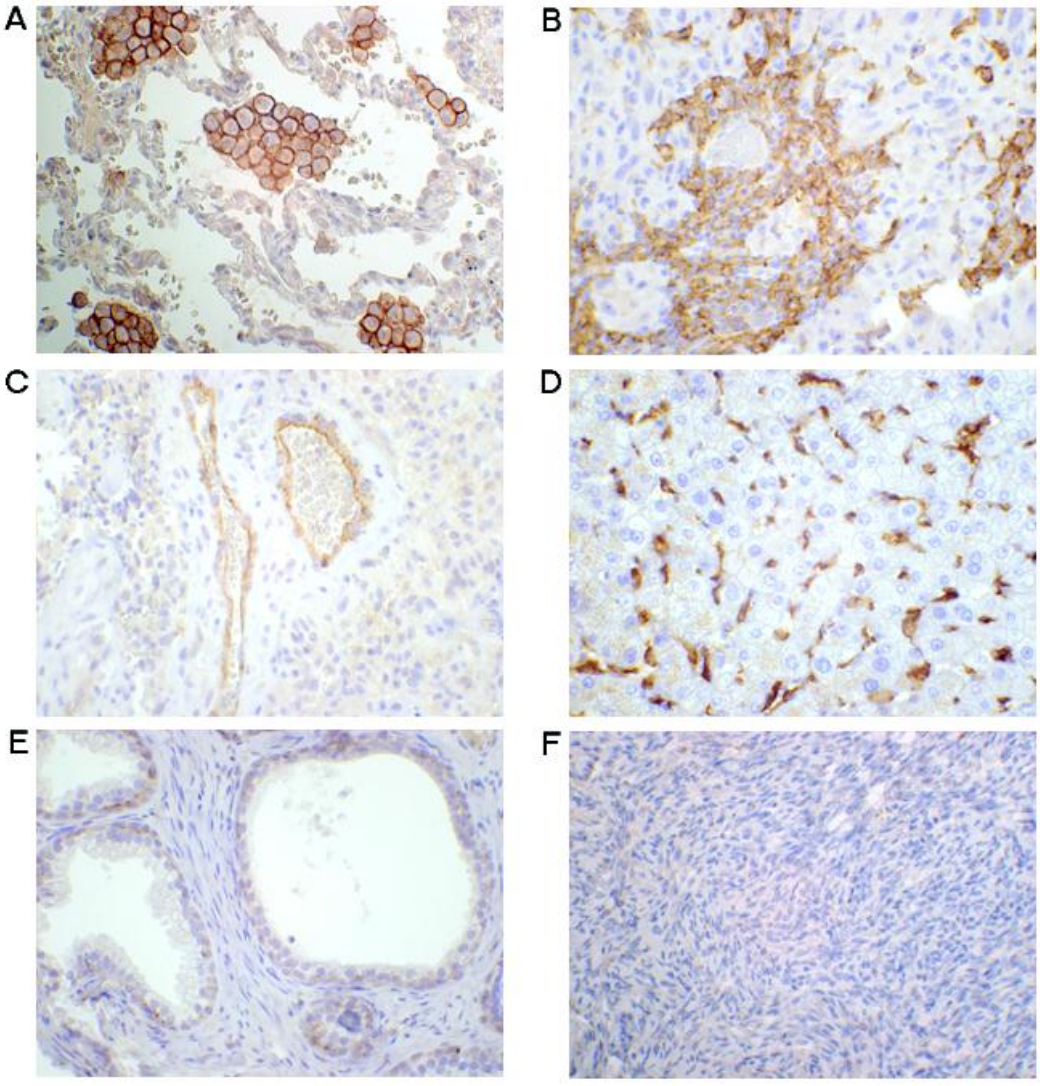

Figure 8: MAb 1H12 staining on FFPE sections of human tissues showing strong membrane staining **(A)** of alveolar macrophages and **(B)** in the lymphohistiocytic host response areas in a melanoma, **(C)** weak staining of the endothelial cells and pericytes in tumour associated vessels in a glioblastoma, **(D)** strong staining in endothelial lining of the sinusoid system and in Kupffer cells of liver, **(E)** weak staining in the basal cells of prostatic glands and **(F)** negative staining of ovarian tissue. All panels show ×400 magnification.

Lavina Ahmed et al, diagnostic pathology 2016, 2:104
ISSN 2364-4893
DOI: http://dx.doi.org/10.17629/www.diagnosticpathology.eu-2016-2:104

Immunohistochemistry on FFPE tumour biopsy samples is another fundamental diagnostic tool. In IHC, MAb 1H12 gave strong and clear membrane staining of Axl-positive FFPE cells compared with other antibodies in our panel, and apparently showed less background staining in non-Axl expressing cells. In a head-to-head comparison of MAb 1H12 with AF154 (commercially available polyclonal antibody widely used for IHC [18, 34]) and MAB154 (commercially available monoclonal antibody used in cryosection by Wienger *et al*., [35]), all three antibodies achieve comparable staining at their optimal concentrations. On FFPE sections from human-in-mouse xenograft models, and on archival human tissue samples (including breast and lung cancer), MAb 1H12 demonstrated good performance with clear signal and low background staining in most cases. Further, the high affinity and long off-rate of MAb 1H12 renders it a 'user-friendly' antibody for IHC use, and it does not require overnight incubation or amplification with an additional secondary antibody and thus requires limited staining time.

Conclusion

In conclusion, MAbs 1H12 and 5F11 represent new anti-human Axl monoclonal antibodies for improved patient biomarker studies. The present findings need to be validated in clinico-pathological studies with larger number of samples.

Abbreviations

Abs: Antibodies

Akt: Protein kinase B

ELISA: Enzyme-linked immunosorbent assay

EMT: Epithelial-to-mesenchymal transition

FFPE: Formalin fixed paraffin embedded

GAPDH: Glyceraldehyde 3-phosphate dehydrogenase

Gas6: Growth arrest specific 6

HCl: Hydrochloric acid

HRP: Horseradish peroxidase

IHC: Immunohistochemistry

MAb: monoclonal antibody

NaCl: Sodium chloride

PBS: Phosphate buffered saline

RFP: Red fluorescent protein

RT: Room temperature

RU: Resonance units

SI: Staining index

SPR: Surface plasmon resonance

TAM: Tyro3, Axl, Mertk

TMA: Tissue microarray

Lavina Ahmed et al, diagnostic pathology 2016, 2:104
ISSN 2364-4893
DOI: http://dx.doi.org/10.17629/www.diagnosticpathology.eu-2016-2:104

Competing Interests

LA, SMK, KWL, HH, JL, LAA, and DRM are employees of, or have a financial stake in, BerGenBio AS (Bergen, Norway), a company developing Axl inhibitors and antibodies. The other authors declare no competing interest.

Authors' contributions

DRM, LAA, JBL conceived, designed and sought funding for this study and revised the manuscript. LA carried out the most laboratory-based work and drafted the manuscript. SK carried out the Biacore experiments and edited the manuscript. HN carried out staining of the patient samples and edited the manuscript. KWL performed the animal experiment. HH made the HRP conjugate of the antibodies. All authors read and approved the manuscript.

Acknowledgments

We thank the Department of Pathology at Haukeland University Hospital for use of archival tissue. We thank Sissel Vik Berge, Ingrid Strand, Gerd Lillian Hallseth, Bendik Nordanger and Randi Hope Lavik for technical support, Gro Gausdal (BerGenBio) for xenograft sections, Dr. Ingeborg M. Bachmann for the melanoma cell lines and Dr. Maria Ramnefjell for her assistance with lung cancer tissues. This work was partly supported by the Research Council of Norway through its Centres of Excellence funding scheme (project number 223250), Industrial PhD program (project number 217076) and BIA programs (project numbers 219701 and 235278).

References

1. Mehlen P, Puisieux A. Metastasis: a question of life or death. Nat Rev Cancer. 2006;6(6):449-58.

2. Thompson EW, Newgreen DF. Carcinoma invasion and metastasis : a role for epithelial-mesenchymal transition? Cancer Res. 2005;65(14):5991-5.

3. Radisky DC. Epithelial-mesenchymal transition. J Cell Sci. 2005;118(19):4325-6.

4. Thiery JP, Sleeman JP. Complex networks orchestrate epithelial-mesenchymal transitions. Nature Rev Mol Cell Biol. 2006;7(2):131-42.

5. Gjerdrum C, Tiron C, Høiby T, Stefansson I, Haugen H, Sandal T, et al. Axl is an essential epithelial-to-mesenchymal transition-induced regulator of breast cancer metastasis and patient survival. PNAS. 2010;107(3):1124-9.

6. Wu X, Liu X, Koul S, Lee CY, Zhang Z, Halmos B. AXL kinase as a novel target for cancer therapy. Oncotarget. 2014;5(20):9546-63.

Lavina Ahmed et al, diagnostic pathology 2016, 2:104
ISSN 2364-4893
DOI: http://dx.doi.org/10.17629/www.diagnosticpathology.eu-2016-2:104

7. Alvarez H, Montgomery EA, Karikari C, Canto M, Dunbar KB, Wang JS, et al. The Axl receptor tyrosine kinase is an adverse prognostic factor and a therapeutic target in esophageal adenocarcinoma. Cancer Biol Ther. 2010;10(10):1009-18.

8. Tsou WI, Nguyen KQN, Calarese DA, Garforth SJ, Antes AL, Smirnov SV, et al. Receptor tyrosine kinases, TYRO3, AXL, and MER, demonstrate distinct patterns and complex regulation of ligand-induced activation. J Biol Chem. 2014;289(37):25750-63.

9. O'Bryan JP, Fridell YW, Koski R, Varnum B, Liu ET. The transforming receptor tyrosine kinase, Axl, is post-translationally regulated by proteolytic cleavage. J Biol Chem. 1995;270(2):551-7.

10. Shieh YS, Lai CY, Kao YR, Shiah SG, Chu YW, Lee HS, et al. Expression of Axl in lung adenocarcinoma and correlation with tumor progression. Neoplasia. 2005;7(12):1058-64.

11. Hutterer M, Knyazev P, Abate A, Reschke M, Maier H, Stefanova N, et al. Axl and growth arrest-specific gene 6 are frequently overexpressed in human gliomas and predict poor prognosis in patients with glioblastoma multiforme. Clin Cancer Res. 2008;14(1):130-8.

12. Shiozawa Y, Pedersen EA, Patel LR, Ziegler AM, Havens AM, Jung Y, et al. GAS6 / AXL axis regulates prostate cancer invasion, proliferation, and survival. Neoplasia. 2010;12(2):116-27.

13. Koorstra J-BM, Karikari CA, Feldmann G, Bisht S, Rojas L, Offerhaus GJ, et al. The Axl receptor tyrosine kinase confers an adverse prognostic influence in pancreatic cancer and represents a new therapeutic target. Cancer Biol Ther. 2009;8(7):618-26.

14. Craven RJ, Xu LH, Weiner TM, Fridell YW, Dent GA, Srivastava S, et al. Receptor tyrosine kinases expressed in metastatic colon cancer. Int J Cancer. 1995;60(6):791-7.

15. He L, Zhang J, Jiang L, Jin C, Zhao Y, Yang G, et al. Differential expression of Axl in hepatocellular carcinoma and correlation with tumor lymphatic metastasis. Mol Carcinog. 2010;49(10):882-91.

16. Rankin EB, Fuh KC, Taylor TE, Krieg AJ, Musser M, Yuan J, et al. AXL is an essential factor and therapeutic target for metastatic ovarian cancer. Cancer Res. 2010;70(19):7570-9.

17. Rochlitz C, Lohri A, Bacchi M, Schmidt M, Nagel S, Fopp M, et al. Axl expression is associated with adverse prognosis and with expression of Bcl-2 and CD34 in de novo acute myeloid leukemia (AML): results from a multicenter trial of the Swiss Group for Clinical Cancer Research (SAKK). Leukemia. 1999;13(9):1352-8.

18. Zhang Z, Lee JC, Lin L, Olivas V, Au V, LaFramboise T, et al. Activation of the AXL kinase causes resistance to EGFR-targeted therapy in lung cancer. Nat Genet. 2012;44(8):852-60.

19. Byers LA, Diao L, Wang J, Saintigny P, Girard L, Peyton M, et al. An epithelial-mesenchymal transition (EMT) gene signature predicts resistance to EGFR and PI3K inhibitors and identifies

Lavina Ahmed et al, diagnostic pathology 2016, 2:104
ISSN 2364-4893
DOI: http://dx.doi.org/10.17629/www.diagnosticpathology.eu-2016-2:104

Axl as a therapeutic target for overcoming EGFR inhibitor resistance. Clinical Cancer Res. 2013;19(1):279-90.

20. Sheridan C. First Axl inhibitor enters clinical trials. Nat Biotechnol. 2013;31(9):775-6.

21. Holland SJ, Pan A, Franci C, Hu Y, Chang B, Li W, et al. R428, a selective small molecule inhibitor of Axl kinase, blocks tumor spread and prolongs survival in models of metastatic breast cancer. Cancer Res. 2010;70(4):1544-54.

22. Ahmed L, Nalwoga H, Arnes JB, Wabinga H, Micklem DR, Akslen LA. Increased tumor cell expression of Axl is a marker of aggressive features in breast cancer among African women. APMIS. 2015;123(8):688-96.

23. Schneider CA, Rasband WS, Eliceiri KW. NIH Image to ImageJ: 25 years of image analysis. Nat Methods. 2012;9(7):671-5.

24. Camp RL, Charette LA, Rimm DL. Validation of tissue microarray technology in breast carcinoma. Lab Invest. 2000;80(12):1943-50.

25. Nocito A, Kononen J, Kallioniemi OP, Sauter G. Tissue Microarrays (TMAS) for high-throughput molecular pathology research. Int J Cancer. 2001;95(1):1-5.

26. Straume OS, Akslen LAA. Alternation and prognostic significance of p16 and p53 protein expression in subgroup of cutaneous melanoma. Int J Cancer. 1997;539:535-9.

27. Barretina J, Caponigro G, Stransky N, Venkatesan K, Margolin AA, Kim S, et al. The Cancer Cell Line Encyclopedia enables predictive modelling of anticancer drug sensitivity. Nature. 2012;483(7391):603-7.

28. Rose AE, Poliseno L, Wang J, Clark M, Pearlman A, Wang G, et al. Integrative genomics identifies molecular alterations that challenge the linear model of melanoma progression. Cancer Res. 2012;71(7):2561-71.

29. Zagórska A, Través PG, Lew ED, Dransfield I, Lemke G. Diversification of TAM receptor tyrosine kinase function. Nat Immunol. 2014;15(10):920-8.

30. Melaragno MG, Fridell Y-WC, Berk BC. The Gas6/Axl system: a novel regulator of vascular cell function. Trends Cardiovasc Med. 2000;9(8):250-3.

31. Strimbu K, Tavel JA. What are biomarkers? Curr Opin HIV AIDS. 2010;5(6):463-6.

32. Linger RMA, Keating AK, Earp HS, Graham DK. TAM receptor tyrosine kinases: biological functions, signaling, and potential therapeutics targeting in human cancer. Adv Cancer Res. 2008;100:35-83.

Lavina Ahmed et al, diagnostic pathology 2016, 2:104
ISSN 2364-4893
DOI: http://dx.doi.org/10.17629/www.diagnosticpathology.eu-2016-2:104

33. Verma A, Warner SL, Vankayalapati H, Bearss DJ, Sharma S. Targeting Axl and Mer kinases in cancer. Mol Cancer Ther. 2011;10(10):1763-73.

34. Ji W, Choi C-M, Rho JK, Jang SJ, Park YS, Chun S-M, et al. Mechanisms of acquired resistance to EGFR-tyrosine kinase inhibitor in Korean patients with lung cancer. BMC cancer. 2013;13(606). doi:10.1186/1471-2407-13-606.

35. Weinger JG, Omari KM, Marsden K, Raine CS, Shafit-zagardo B. Up-regulation of soluble Axl and Mer receptor tyrosine kinases negatively correlates with Gas6 in established multiple sclerosis lesions. Am J Pathol. 2009;175(1):283-93.

Additional files

Additional file 1: Table S1.

IHC staining on cryosections of normal human tissues with MAb 1H12. Triplicate samples from 30 different tissues were included in the study. Staining intensity was judged as negative (0), weak reaction (1+), moderate reaction (2+), or strong reaction (3+). Format: doc, Size: 47KB.

Additional file 2: Figure S1.

Pattern of Axl staining in the A549 cell line pellets in relation to duration of formalin fixation. (**A**) 12 hours, staining was good enough for adequate evaluation within 12 hours of fixation: strong membrane expression in a few cells and weak expression in majority of cells; (**B**) 24 hours, optimal specific membrane staining: moderate-strong Axl expression in majority of cells; (**C**) 48 hours, (**D**) 5 days and (**E**) 1 week specific membrane staining is still adequate; (**F**) 2 weeks, weak specific membrane expression in majority of cells while more cells show negative expression than at shorter fixation periods. All panel show ×630 magnification. Format: doc, Size: 1.34MB.